

AD 717984

RELATION BETWEEN PARTICULATE CHEMISTRY AND CERAMIC PROPERTIES

ANNUAL REPORT

1 January 1970 - 31 December 1970

Contract N00014-70-C-0138

AVSD-0024-71-CR

Prepared by

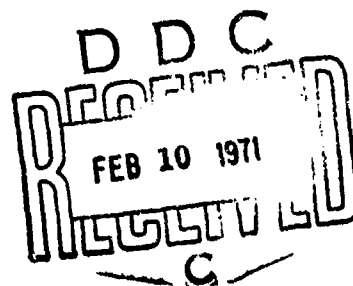
W.H. Rhodes  
B.J. Wuensch  
T. Vasilcs

Prepared for

Office of Naval Research  
Washington, D.C. 20360

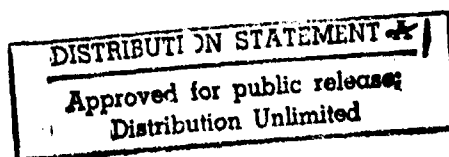
Submitted by

AVCO CORPORATION  
Systems Division  
Lowell, Massachusetts 01851



Reproduction in whole or in part is permitted for any purpose of the U.S. Government. Distribution of this document is unlimited.

Reproduced by  
NATIONAL TECHNICAL  
INFORMATION SERVICE  
Springfield, Va. 22151



RELATION BETWEEN PARTICULATE CHEMISTRY AND CERAMIC PROPERTIES

ANNUAL REPORT

1 January 1970 - 31 December 1970

Contract N00014-70-C-0138

AVSD-0024-71-CR

Prepared by

W.H. Rhodes  
B.J. Wuensch  
T. Vasilos

Prepared for

Office of Naval Research  
Washington, D.C. 20360

Submitted by

AVCO CORPORATION  
Systems Division  
Lowell, Massachusetts 01851

Reproduction in whole or in part is permitted for any purpose of the U.S. Government. Distribution of this document is unlimited.

## FOREWORD

This report was prepared by the Systems Division of Avco Corporation under U.S. Navy Contract N00014-70-C-0138 entitled, "Relation Between Particulate Chemistry and Ceramic Properties".

The work was administered under the direction of Dr. Arthur Diness, Office of Naval Research.

This report covers work conducted from 1 January 1970 to 31 December 1970.

The authors are pleased to acknowledge the contributions of the following individuals to the program: J. Centorino and J. Zgrebnak for materials preparation, R. Gardner and P. Fuce for ceramographic preparation, C.L. Houck for electron microscopy and P. Bernsburg for x-ray studies.

## ABSTRACT

Progress is described in the first year of a program designed to examine the relation of mechanical properties, grain-growth kinetics and impurity precipitate distribution to the characteristics and chemistry of initial MgO particulates at progressive stages during microstructure evolution. Efforts have concentrated on production of an ultrapure, fully dense microstructure which will form the standard with which subsequent experiments with doped particulates will be compared. Magnesium oxide vacuum hot pressed specimens were prepared from static and dynamically calcined high purity ( $\geq 99.99\%$  MgO)  $\text{Mg}(\text{OH})_2$  and  $\text{MgCO}_3$  powders. Microstructure development was studied at stages in the calcining and consolidation processes and it was learned that abnormal grain-growth begins at the 70% density level in  $\text{Mg}(\text{OH})_2$  derived material. Crystallites are crystallographically oriented to one another and form an agglomerate which is a relic of the brucite crystal and have very rapid grain-growth rates. Fully dense 1150°C hot pressed specimens had a marked duplex structure, but pressing at 1450°C resulted in material with a normal grain distribution. This unusual reversion from abnormal back to normal grain distribution was probably due to competition between boundary and pore control on grain growth. Slight introduction of Fe and Zn occurred during consolidation, but Cl, S and Na volatilize and the total impurity content of the compacts is less than that of the starting material.  $\text{MgCO}_3$  derived material resulted in normal grain distributions when pressed at 1150°C but abnormal grain size distributions developed at higher temperatures.

Grain growth studies were performed at two temperatures on  $\text{Mg}(\text{OH})_2$  derived material having a normal grain size distribution. The growth rate decayed well beyond the normal square dependence due to the transition from boundary control to pore control and then to abnormal grain growth resulting from the critical relations between grain size and pore size (the 0.1 to 0.4% porosity only became apparent during the anneals). A discussion and explanation of the various grain growth studies in MgO is included.

TABLE OF CONTENTS

FOREWORD

ABSTRACT

I.	INTRODUCTION. . . . .	1
II.	OBJECTIVES OF THE PRESENT PROGRAM . . . . .	1
III.	THEORY AND PREVIOUS RESULTS . . . . .	2
	3.1 Theories of Grain Growth . . . . .	2
	3.2 Previous Results for Magnesia. . . . .	3
IV.	PROGRAM PROGRESS. . . . .	4
	4.1 Powder Preparation . . . . .	4
	4.2 Consolidation. . . . .	13
	4.3 Chemical Analysis. . . . .	16
	4.4 Grain Growth . . . . .	20
	4.5 Discussion . . . . .	20
V.	CONCLUSIONS . . . . .	25
VI.	REFERENCES. . . . .	26

LIST OF ILLUSTRATIONS

Figure No.

1	Electron Micrograph of High Purity $Mg(OH)_2$ Powder. . .	5
2	Electron Diffraction Patterns of Brucite Single Crystal Decomposition in the Electron Beam, a) initial pattern, b) 20 seconds exposure, and c) after 40 second exposure. . . . .	6
3	Structure of MgO Crystallite within a Relic of a Brucite Platelet after Calcination at (a) $375^{\circ}C$ , 55 Minutes and (b) $375^{\circ}C$ , 180 Minutes. . . . .	7
4	MgO Calcined from $Mg(OH)_2$ in Rotary Vacuum Calciner at (a) $800^{\circ}C$ -1 hr., (b) $1000^{\circ}C$ -1 hr., and (c) $1200^{\circ}C$ -1 hr. . . . .	9
5	MgO Calcined from $MgCO_3$ in Rotary Vacuum Calciner at (a) $800^{\circ}C$ -1 hr., (b) $1100^{\circ}C$ -1/2 hr., and (c) supplied by Honeywell (calcining conditions unknown). . . . .	10
6	Crystallite Size Distribution for High Purity MgO Powder $Mg(OH)_2$ Calcined $1200^{\circ}C$ , 1 Hour . . . . .	11
7	Microstructure of Three High Purity MgO Hot Pressed Specimens Pressed from $Mg(OH)_2$ Derived Powder after Various Hot Pressing Cycles. . . . .	14
8	Microstructure of Three High Purity MgO Hot Pressed Specimens from $Mg(OH)_2$ Derived Powder after Various Powder Calcining Cycles. . . . .	15
9	Microstructure Evolution of $Mg(OH)_2$ Derived MgO at (a) 69% Density, (b) 92.5% Density, and (c) 99.5% Density. . . . .	17
10	Microstructure of Two MgO Samples Produced from $MgCO_3$ Derived Powder . . . . .	18
11	Grain Growth in High Purity MgO and Comparison with Literature Values. . . . .	21
12	Microstructure after Approximately 1000 Minutes Annealing at (a) $1300^{\circ}C$ , (b) $1525^{\circ}C$ , and (c) $1610^{\circ}C$ . .	22

LIST OF TABLES

Table No.

I	MgO Crystallite for Various Calcination Treatments. . . . .	12
II	Impurity Analysis for Magnesia Base Powder Lots and a Fabricated Sample . . . . .	19

## I. INTRODUCTION

Polycrystalline bodies are involved in nearly all applications of ceramics. Many of the useful properties of such materials are controlled by grain size and grain boundary properties. The relationship between grain size and mechanical properties, for example, has long been known. Equally important, however, is the physical and chemical state of the grain boundaries in the material. It has been only recently appreciated that impurities in ceramics are commonly segregated at grain boundaries even when present in concentrations as low as 30 ppm.<sup>1</sup> Boundary sensitive properties may thus be completely dominated by impurities even in samples whose bulk composition indicates a fairly high purity.

Impurity segregation may influence ceramic properties at two levels. First, many aspects of the behavior of ceramics depends directly on the physical state of the boundaries. Segregation may give rise to enhanced mass transport at grain boundaries<sup>2</sup> and thus completely modify the kinetics of processes such as creep, oxidation, electrical conduction and sintering. Segregation is similarly known to directly affect strength and mechanical behavior.<sup>3</sup> On a second level, impurity segregation influences microstructure development and thus, through its influence during processing, may control final properties which are dependent upon microstructure. An example is the intentional addition of small amounts of impurity to retard grain growth during sintering. This prevents the entrapment of pores within grains and thereby has permitted sintering of oxides to full theoretical density.

Few studies of boundary-sensitive properties have adequately characterized the physical and chemical state of grain boundaries. Consequently, little is known of the relation between the chemistry of the initial particulates from which a ceramic body is formed, and the impurity distribution in the final microstructure. Similarly, little is known of how impurity precipitate size and distribution changes during the course of microstructure evolution, or the manner in which such changes influence properties. Such questions are difficult to answer since a grain boundary is essentially a two-dimensional structure. The volume of material affected, and the amounts of impurity involved may thus be very small. Recently developed tools - notably scanning spectroscopy, electron microbeam probe spectroscopy, and electron microscopy provide promising means for gaining insight into such problems.

## II. OBJECTIVES OF THE PRESENT PROGRAM

The present report is the first Annual Report in a program designed to examine the inter-relation of mechanical properties, grain-growth kinetics and impurity precipitate distribution with the characteristics and chemistry of the initial particulates at progressive stages during the evolution of a ceramic microstructure. Magnesium oxide has been selected for study for a number of reasons. This material is of considerable technological importance (e.g., as a refractory, use as transparent armor, and in high temperature infrared applications). Several measurements of grain-growth kinetics have been made for this material<sup>4-7</sup> which are not in complete accord. Clarification of these measurements with a well-characterized magnesia is badly needed. Further, extensive data are available for the rates of diffusion of several of

the impurity cations commonly present in commercial-grade MgO.<sup>8</sup> Such data will be of value in the interpretation of the rates of impurity segregation and redistribution.

The specific aims of this program are eventual

- 1) Preparation and characterization of ultrapure MgO particulates and also particulates which have been homogeneously doped with controlled amounts of impurity,
- 2) Consolidation of the particulates into initial bodies which are pore-free and have both a fine and uniform grain size,
- 3) Measurement of isothermal grain-growth kinetics for both ultrapure and doped materials,
- 4) Determination of impurity precipitate concentration and distribution at successive stages of microstructure evolution, and
- 5) Correlation of mechanical properties with precipitate distribution and microstructure.

As reviewed in the following section, the results of previous studies of magnesia differ. The disparities are undoubtedly due to impurity effects and minor levels of porosity. Accordingly, the first year's effort in the present program was primarily concerned with the production and characterization of fine ultrapure MgO particulates, and their consolidation into a fully-dense controlled microstructure. Such samples must serve as the standard microstructure with which subsequent experiments with doped materials will be compared. Progress is described in Section IV.

### III. THEORY AND PREVIOUS RESULTS

#### 3.1 Theories of Grain Growth

Normal grain growth describes a process in which the average grain size of a strain-free material increases continuously with time at elevated temperature without appreciable change in the distribution of grain sizes. The driving force is the difference in energy between large- and fine-grained material which results from reduction of grain-boundary area. In contrast, discontinuous or abnormal grain growth is a process in which a few large grains grow at the expense of a fine-grained matrix.

For normal grain growth in a pure, fully dense system, a theory due to Turnbull predicts

$$D^2 - D_0^2 = (K \gamma V) t \quad (1)$$

where  $D$  is average grain diameter,  $D_0$  is initial grain diameter,  $K$  is a rate constant,  $\gamma$  is interfacial energy,  $V$  is molar volume, and  $t$  is time.

In non-ideal systems either the migration rate of pores<sup>10,11</sup>, the diffusion of solid solution impurities<sup>12</sup> ("impurity drag"), or precipitation of second phase may control grain-growth kinetics. Brook<sup>14</sup> has considered the microstructural conditions for which each effect might be expected to be dominant. His results show that control by boundary mobility is to be expected when pores are small. Separation of boundaries from pores (pore entrapment), is to be expected when the pore velocity becomes less than the boundary velocity and will occur at large grain sizes and when the pores are large and widely dispersed. Porosity-controlled grain-growth occurs at small grain sizes and when the pores are large and close together. The effect of impurity is to increase the mobility of pores relative to that of the boundary and thus, for a given grain size, increase the boundary-controlled region of behavior at the expense of the pore entrapment region.

### 3.2 Previous Results for Magnesia

Several studies of grain growth in magnesia have been conducted, but the influence of porosity and impurity on the process is not clear. Measurements by Daniels et al<sup>4</sup> were among the first to be conducted on a ceramic oxide. The data indicated normal grain growth, but the measurements were complicated by the presence of considerable porosity and attendant densification during annealing of the specimens. Subsequent measurements at Avco<sup>5</sup> were the first to be conducted with a fully dense oxide. The kinetics of normal grain growth were again observed but, in the absence of porosity, growth rates were 4 to 6 times more rapid. Addition of 1% Fe or Ti impurity to magnesia<sup>6</sup> produced grain growth rates much smaller than those observed in earlier studies of either the porous<sup>4</sup> or fully-dense compacts<sup>5</sup> and, further, a change to a time dependence of  $1/4$  and  $1/3$  for the Fe and Ti additions, respectively.

A detailed study of grain growth in pure and Fe<sub>2</sub>O<sub>3</sub>-doped magnesia with objectives similar to, but not identical with, the present work was reported by Gordon et al<sup>7</sup> midway through the present study. Their results may be summarized as follows. Pure MgO did not exhibit the  $t^2$  dependence of earlier studies, but exhibited an exponent which decreased with time. Grain growth was probably controlled by porosity in pure magnesia at all temperatures even though the amounts of porosity were small (less than 1%). The addition of Fe<sub>2</sub>O<sub>3</sub> decreased the rate of grain growth and tended to stabilize normal grain growth kinetics.

From the above, it appears that early results, in which normal grain growth kinetics were observed, represent experiments in which microstructure evolution was controlled by impurities. In high purity specimens, samples of full theoretical density are required if kinetics are not to be dominated by porosity. Preparation of the starting materials with the requisite fine grain size will be difficult since, in the absence of porosity and impurities, the initial grain growth is expected to be very rapid. Experience in the present program has borne this out. While the presence of impurities has been demonstrated to retard grain growth kinetics, the redistribution and state of the impurities as the microstructure evolves has yet to be examined and interpreted in terms of impurity diffusion rates.

#### IV. PROGRAM PROGRESS

##### 4.1 Powder Preparation

Successful consolidation studies require a highly reactive powder which, of course, usually dictates that the average particle size is submicron. Several years ago a detailed search of commercial MgO powder suppliers failed to reveal a source of high purity ( $\geq 99.99\%$  MgO) submicron MgO. However, high purity  $Mg(OH)_2$  and  $MgCO_3$  were available. Thus, careful control of the calcination process could in theory produce the desired starting powder. Fabrication studies were performed on powders calcined from  $Mg(OH)_2$  and a renewed effort to locate commercial submicron high purity MgO powder was initiated.

The  $Mg(OH)_2$ \* powder was characterized by x-ray diffraction and electron microscopy techniques. The powder was shown to be brucite,  $Mg(OH)_2$ , and Figure 1 illustrates the plate-like morphology of the starting powder. The calcination to MgO was studied by performing both static and dynamic calcinations and examining the morphology in the electron microscope. Also, brucite was decomposed in the electron beam and the development of the MgO crystallite was directly observed. This latter effort will be discussed first.

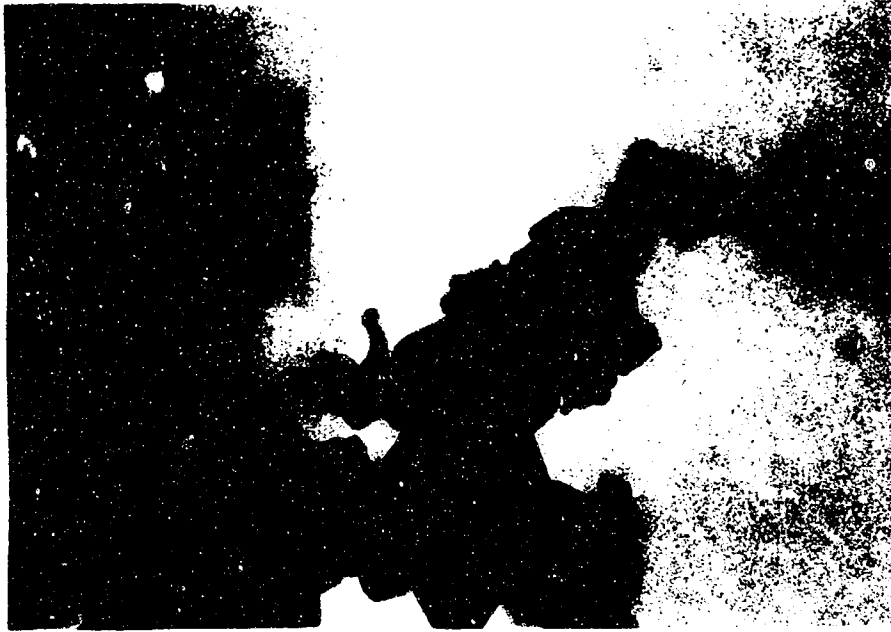
Figure 2 shows diffraction patterns recorded during actual decomposition of a brucite platelet. In the initial diffraction pattern (Figure 2a), the (110) prismatic planes and (100) type planes for brucite are present. The (220) reflections for periclase are missing, but other MgO diffraction spots are present. After 20 seconds of beam heating (Figure 2b), the (220) magnesium oxide spots appeared on the same radius vectors as the (110) brucite reflections. However, the (100) and (110) brucite reflections were still visible. Upon further heating, a more distinct separation was observed between the magnesium oxide reflections and the brucite spots. The brucite spots gradually diminished in intensity until only the periclase single crystal pattern remained having a  $[111]$  zone axis (Figure 2c).

Powders were statically calcined in a 2 mm deep bed under a partial vacuum at several temperature and times. Initially suitable temperatures and times were selected from the kinetics of studies of Gordon and Kingery.<sup>12</sup>

Calcination at  $375^\circ C$  for 55 minutes resulted in agglomerates up to 10 microns and individual multi-crystal platelets of 0.8 microns (Figure 3a). X-ray line broadening demonstrated that MgO particle size was in the 100 angstrom size range and, indeed, a high magnification examination of a platelet revealed this size MgO crystallite within a relic of the original brucite platelet. Holding the calcination at  $375^\circ C$  for 180 minutes (Figure 3b) resulted in a rod-like shape. This suggests that oriented growth of MgO occurs. Some of the small MgO particles fractured apart possibly from strain associated with the nucleation and growth process. With this tendency for oriented growth, it would appear to be desirable to break down the relic brucite structure prior to hot pressing or sintering. If this is not accomplished it is quite possible that equiaxed microstructures would be extremely difficult to produce.

---

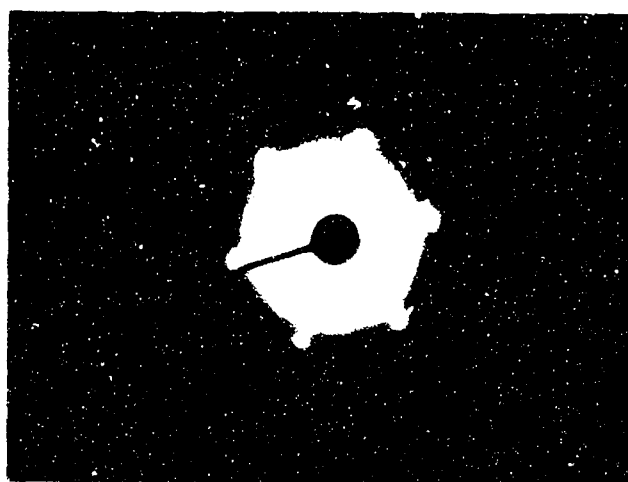
\* Purchased from Johnson-Matthey through United Mineral Corp. (U.S. Distributors).



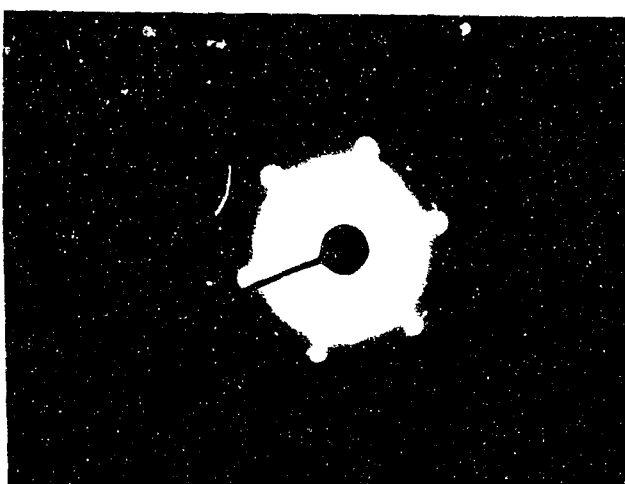
#67050

90,000X

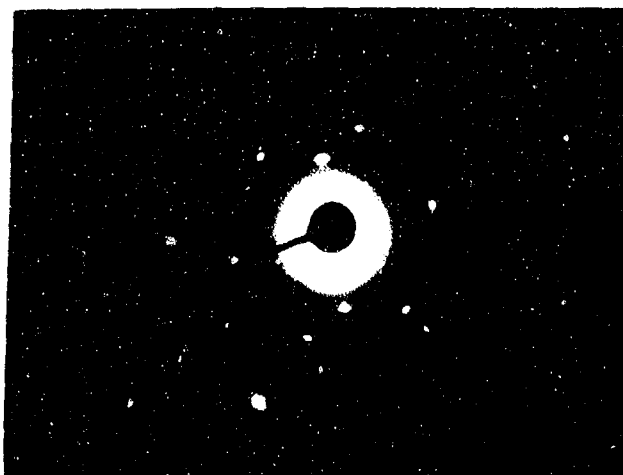
Figure 1. Electron Micrograph of High Purity  $\text{Mg}(\text{OH})_2$  Powder.



a

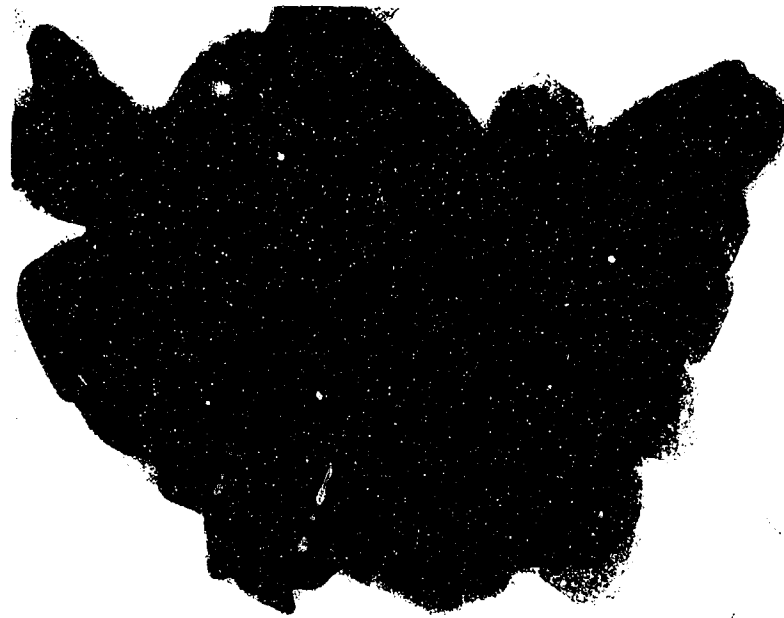


b



c

Figure 2. Electron Diffraction Patterns of Brucite Single Crystal Decomposition in the Electron Beam, a) initial pattern, b) 20 seconds exposure, and c) after 40 second exposure.



#67661

a

120,000X



#68141

b

60,000X

Figure 3. Structure of MgO Crystallite within a Relic of a Brucite Platelet after Calcination at (a) 375°C, 55 Minutes and (b) 375°C, 180 Minutes.

The initial process studies resulted in a duplex microstructure, and one interpretation for the results was centered on a strong influence of retained  $\text{OH}^-$  on microstructure development. This combined with a desire to break up agglomerates led to the construction of a dynamic calcining apparatus. The  $\text{Mg}(\text{OH})_2$  powder was held within a new platinum cylinder reserved for this program and it in turn was positioned within a closed end high purity alumina tube. This tube was positioned at a  $20^\circ\text{C}$  incline and was rotated at 2 rpm and evacuated during calcinations up to  $1200^\circ\text{C}$ .

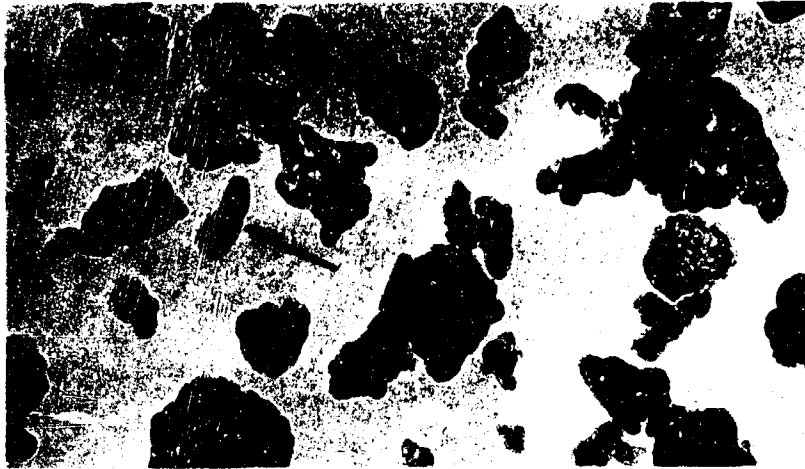
A series of calcinations were conducted at temperatures greatly in excess of those required to decompose brucite. Figure 4 illustrates the crystallite structure over the range of conditions employed. Figure 4a illustrates a disc-shaped agglomerate with very tight packing of crystallites and a mean crystallite size of 260 Å. Calcining  $200^\circ\text{C}$  higher,  $1000^\circ\text{C}$ , developed cube crystallites still tightly packed into agglomerates. The agglomerates are no longer disc-shaped as some fracturing appears to have taken place. One or two agglomerates (arrow) appear to have sintered into a tight large crystal (these may have retained some of their polycrystallinity but they are certainly seeds for secondary grain growth). The highest temperature employed,  $1200^\circ\text{C}$ , developed the crystallite size to 360 Å and continued the development of a cubic habit. Further, the crystallites within an agglomerate appear to be crystallographically oriented to each other. This creates boundaries within an agglomerate that are "special" and may well have quite different grain boundary migration rates than non-oriented boundaries which are present in some agglomerates but more commonly occur between crystallites from adjacent agglomerates.

Two dynamic calcination runs were conducted with reagent grade  $\text{MgCO}_3^*$  and the resultant structures are illustrated in Figure 5. Also shown is a micrograph of  $\text{MgO}$  powder purchased from Honeywell who in turn calcined the powder from a second reagent grade of  $\text{MgCO}_3^{**}$ . The agglomerates are much larger for the  $800^\circ\text{C}$ -1 hr. calcine than they were for material calcined from  $\text{Mg}(\text{OH})_2$ . The agglomerates are much more open; that is, a greater space appears between crystallites. Figure 5b illustrates the development of a cube crystal habit, as was the case for higher temperature calcined from  $\text{Mg}(\text{OH})_2$ . The individual crystallites within an agglomerate do not appear to be crystallographically oriented to each other. The Honeywell material illustrated in Figure 5c possesses a larger crystallite size than any of the other  $\text{MgO}$  powders calcined in this program; however, the agglomerates appear somewhat smaller and more loosely packed than the rotary calcinations of  $\text{MgCO}_3$ .

The distribution of crystallite sizes was examined for the  $1200^\circ\text{C}$ -1 hr calcination. The data plotted on log-normal probability paper yield a straight line (Figure 6) indicative of a log-normal distribution which is expected for normal nucleation and growth. Table I gives the mean crystallite size for the various calcination treatments tested in this program. This data was analyzed by plotting mean crystallite versus log time where applicable and log diameter versus reciprocal temperature. As can be observed from examination of the table, the growth kinetics are exceedingly slow with an activation energy of only 0.78 e.V. The self-diffusion activation energies; 3.43 eV for

\* Fisher Chemical Co.

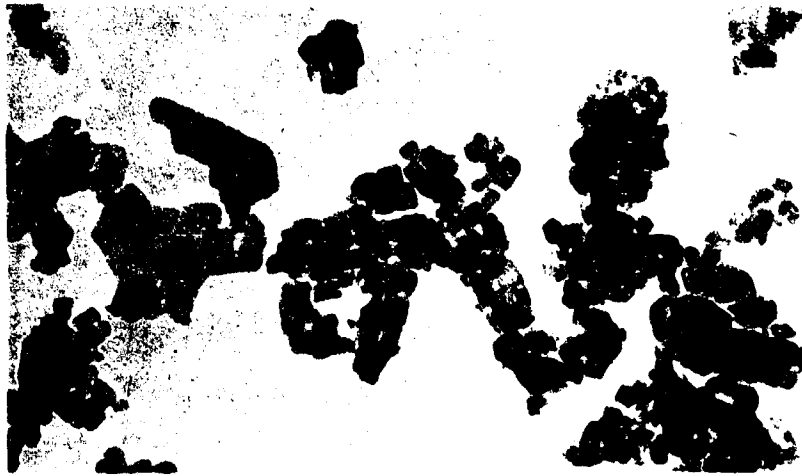
\*\* Mallinckrodt.



#70604A

a

80,000X



#70610A

b

80,000X

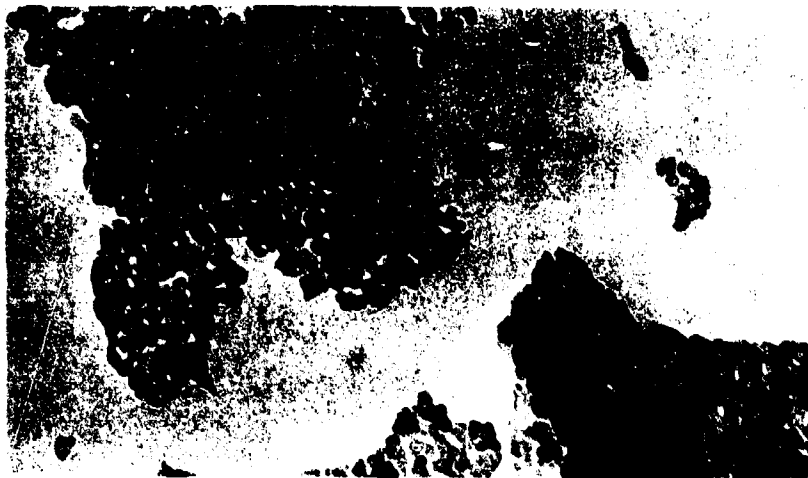


#70628B

c

80,000X

Figure 4. MgO Calcined from  $Mg(OH)_2$  in Rotary Vacuum Calciner at (a)  $800^\circ C$ -1 hr., (b)  $1000^\circ C$ -1 hr., and (c)  $1200^\circ C$ -1 hr.



#70651A

a

80,000X



#70654B

b

80,000X



#70657B

c

80,000X

Figure 5. MgO Calcined from  $MgCO_3$  in Rotary Vacuum Calciner at (a)  $800^{\circ}C$ -1 hr., (b)  $1100^{\circ}C$ -1/2 hr., and (c) supplied by Honeywell (calcining conditions unknown).

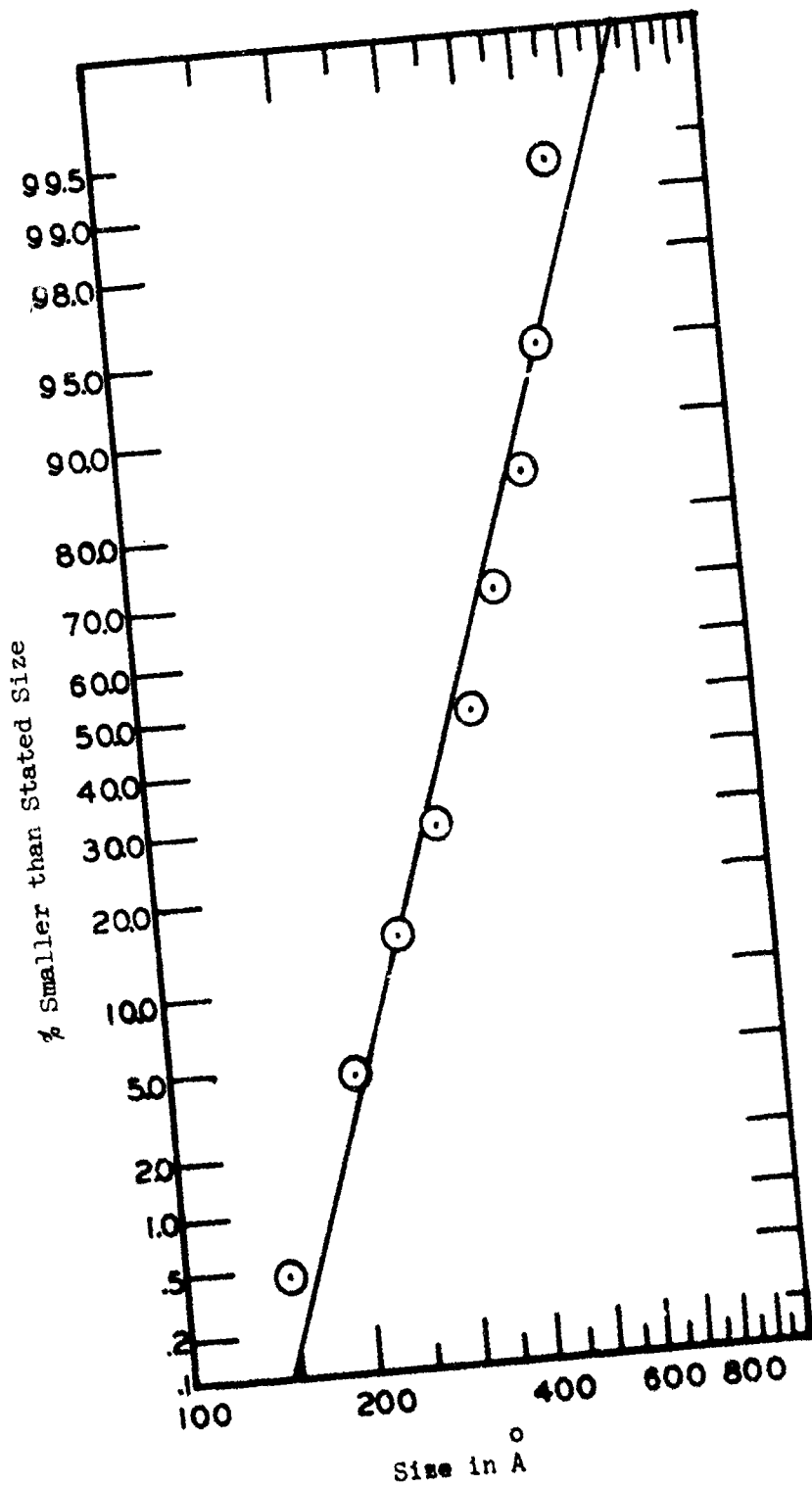


Figure 6. Crystallite Size Distribution for High Purity MgO Powder  $\text{Mg}(\text{OH})_2$  Calcined  $1200^\circ\text{C}$ , 1 Hour.

TABLE I

MgO CRYSTALLITE FOR VARIOUS CALCINATION TREATMENTS

<u>Starting Compound</u>	<u>Lot No.</u>	<u>Condition</u>	<u>Temperature</u>	<u>Time</u>	<u>Mean Crystallite Size</u>
Mg(OH) <sub>2</sub>	SH194*	Static	350	55	~100
	SH194	Static	375	55	~100
	SH182	Static	375	180	~100
	SH194	Static	375	180	~100
	SH182	Static	800	60	450
	SH182	Dynamic	800	60	260
	SH182	Dynamic	900	60	263
	SH182	Dynamic	1000	60	278
	SH182	Dynamic	1100	30	288
	SH182	Dynamic	1100	60	293
	SH182	Dynamic	1100	120	299
	SH182	Dynamic	1200	10	333
	SH182	Dynamic	1200	30	358
	SH182	Dynamic	1200	60	363
	MgCO <sub>3</sub>	700752**	Dynamic	800	60
700752		Dynamic	1100	30	318

\* Johnson-Matthey

\*\*Fisher

$Mg^{2+}$  and 2.71 eV for  $O^{2-}$ , are significantly higher indicative that some other process than lattice self-diffusion controlling the powder growth process. Suggested limiting mechanisms include diffusion across grain boundaries or dynamics of the rotating powder bed. The fact that the crystallites from the static 800°C calcine were about twice as large as from the dynamic calcine undergoing the same thermal history strongly suggests the latter as the limiting step. Because of the low growth rate, a number of calcination runs were conducted at 1200°C for 1 hour giving a very fine particulate powder where a high degree of decomposition and volatilization of  $OH^-$  could be realized.

#### 4.2 Consolidation

Vacuum hot pressing techniques were employed for densification. High strength\* graphite dies were employed which allowed pressing up to 15,000 psi. The powder was loaded into the die under static air glove box conditions, placed into the assembly and lightly cold pressed. After evacuation the sample was heated to 800°C without pressure to allowed continued outgassing. At this point, pressure application was continued while temperature was increased until both desired parameters were achieved. The time of pressure application was in part governed by past experience and also guided by the deflection rate. Typical vacuums at peak temperature were in the order of  $1 \times 10^{-4}$  mm Hg.

An initial series of specimens were hot pressed using powder calcined statically at 375°C for 180 minutes. Three structures representative of samples hot pressed at three different temperatures, are shown in Figure 5. A hierarchy of fine grains is apparent in Figure 7a and these are also present, but in a smaller concentration, in Figure 7b. However, Figure 7c shows a complete absence of this fine-grained population. The main and probably controlling variable in achieving these three distinctly different microstructures was the hot pressing temperature. Increased hot pressing temperature favored the development of more uniform microstructures. It is particularly noteworthy that this decreased concentration of fine-grains did not necessarily require increased matrix grain intercept size (Figure 7a, grain size is 21  $\mu m$  and Figure 7b, grain is 15  $\mu m$ ).\*\* Thus, temperature is critical to the evolution of the fine-grain material to large equiaxed grains.

The duplex microstructure was clearly undesirable from the standpoint of subsequent property or grain growth studies. It was hypothesized that high temperature dynamic calcining would, 1) reduce the concentration of volatiles, and 2) break down agglomerates where either effect might reduce the tendency for duplex grain development. Further, it was desirable to achieve fine microstructures ( $< 10 \mu m$  grain intercept) for grain growth studies as growth is difficult to measure on large-grained material except at very high temperatures. A series of hot pressings were conducted with powders calcined under a variety of conditions outlined in Table I. Representative microstructures are illustrated in Figure 8. Again, the hierarchy of fine grains was observed. None of the calcining conditions gave the desired microstructures.

---

\* Poco Graphite Co.

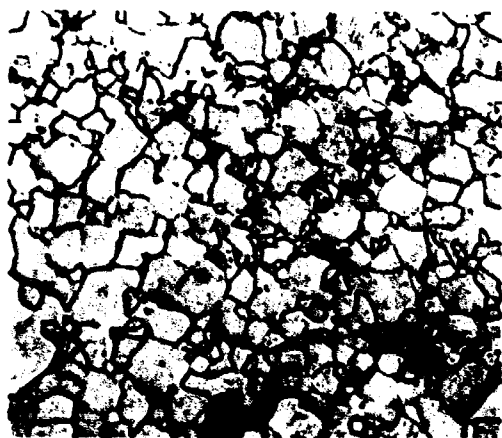
\*\* This inversion of grain size with increasing thermal history is surprising and unexplained.

Hot Pressing Conditions  
and Results

SH182 -  $Mg(OH)_2$   
180 min. static powder calcine  
375 °C.  
1150 °C - 15 Kpsi - 90 min.  
3.565 gm/cc - 21  $\mu m$  grain intercept

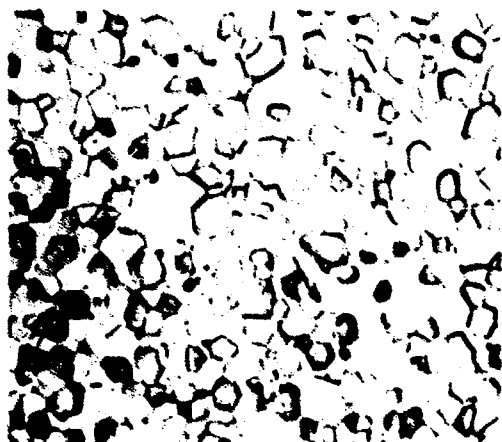


#5014-1 (a) 100X



#4984 (b) 250X

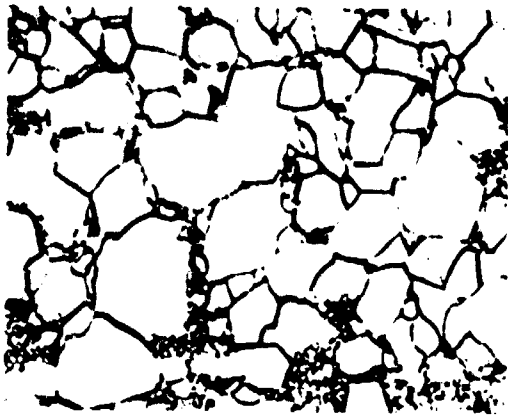
SH182  $Mg(OH)_2$   
375 °C - 180 min. static powder  
calcine  
1200 °C - 15 Kpsi - 115 min.  
3.580 gm/cc - 15  $\mu m$  grain intercept



#839-D (c) 75X

SH194 -  $Mg(OH)_2$   
375 °C - 180 min. static powder  
calcine  
1450 °C - 8 Kpsi - 112 min.  
3.583 - 40  $\mu m$  grain intercept

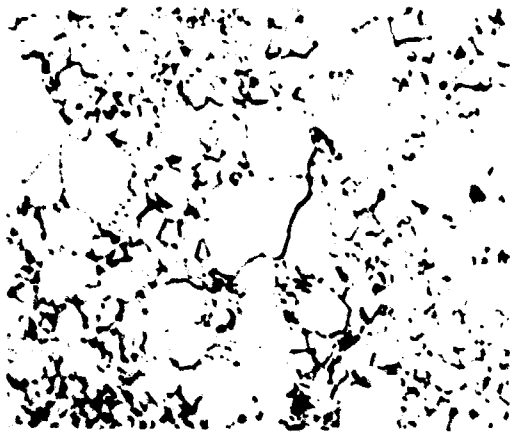
Figure 7. Microstructure of Three High Purity MgO Hot Pressed Specimens Pressed from  $Mg(OH)_2$  Derived Powder after Various Hot Pressing Cycles.



#5331-2 a 750X

Hot Pressing Conditions  
and Results

SH194  $Mg(OH)_2$   
800°C - 60 min. static calcine  
1150°C - 15 Kpsi - 115 min.  
3.569 gm/cc - 10  $\mu m$  grain intercept



#5405-3 b 750X

SH182  $Mg(OH)_2$   
1200°C - 60 min. dynamic calcine  
1155°C - 15 Kpsi - 90 min.  
3.586 gm/cc - 6  $\mu m$  grain intercept



#5412-4 c 750X

SH162  $Mg(OH)_2$   
1200°C - 60 min dynamic calcine  
1255°C - 15 Kpsi - 30 min.  
3.601 gm/cc - 16  $\mu m$  grain intercept

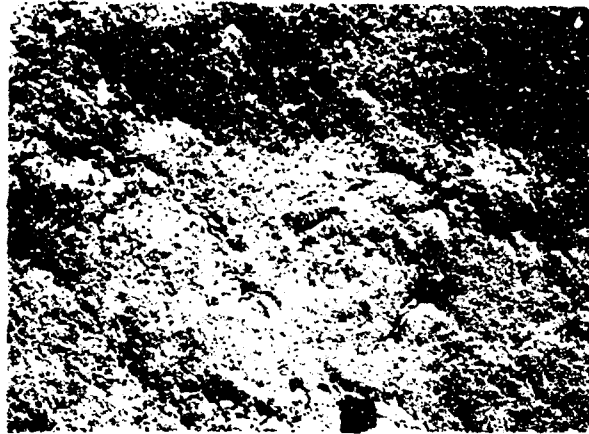
Figure 8. Microstructure of Three High Purity MgO Hot Pressed Specimens Pressed from  $Mg(OH)_2$  Derived Powder after Various Powder Calcining Cycles.

The evolution of the duplex microstructure was studied by deliberately terminating several fabrication cycles at intermediate levels of density. The microstructures were studied by a combination of light and electron microscopy techniques. Representative electron micrographs are shown in Figure 9. The sample in Figure 9a is 69% dense. The pores appear to be located primarily at triple-point grain intersections. In general, the grain size appears to be about 0.3  $\mu\text{m}$ . However, even at this point there are many grains far outside the expected normal distribution of grain sizes; namely, about 0.5  $\mu\text{m}$ . Figure 9b illustrates the structure of 92.5% density. The densification appears to be non-uniform with 0.1 cm lens-shaped regions of high density (arrow A) having a smaller grain size (0.3  $\mu\text{m}$ ) than the matrix and patches (arrow B) of low density with a grain size (0.5  $\mu\text{m}$ ) about equal to the matrix. The pores in the low density area have a similar morphology to those from the low density sample. The 99.5% dense sample shown in Figure 9c exhibits the strong duplex grain structure. The fine-grains are now 1  $\mu\text{m}$  and the large grains are now in the 30  $\mu\text{m}$  range. Some porosity (arrow C) is associated with the fine-grain size area. Thus, it is apparent that the duplex microstructure evolves during the initial stages of densification. Also, there are zones of varying density during the cycle which may contribute to the non-uniform structure but are probably not the main cause. These aspects will be discussed in more detail in Section 4.5.

A number of fabrication runs were conducted with Honeywell MgO powder. Representative microstructures are shown in Figure 10. The polished sections of both samples exhibited little porosity; however, the amount present was concentrated in 200  $\mu\text{m}$  spherical regions. The sample illustrated in Figure 10 had a 0.5  $\mu\text{m}$  grain size requiring electron microscopy techniques to resolve the etched structure. The etching has severely attacked the grain boundaries, thus, it is not possible to identify any residual porosity. It is especially noteworthy that the grain size is about 30 times smaller than experienced for  $\text{Mg}(\text{OH})_2$  derived powder processed by the same cycle. Hot pressing the Honeywell powder at a higher temperature (Figure 10b) increases the grain intercept to 6  $\mu\text{m}$  and some tendency exists for an abnormal grain size distribution. The grain intercept is still  $\sim 30 \mu\text{m}$  less than would be expected for the  $\text{Mg}(\text{OH})_2$  derived MgO (see Figure 7c).

#### 4.3 Chemical Analysis

The suppliers chemical analysis for the two lots of  $\text{Mg}(\text{OH})_2$  and a typical analysis<sup>16</sup> for Honeywell MgO are given in Table II. Lot SH194 in particular, represents an extremely clean analysis. Samples produced from Lot SH182 were analyzed on an earlier program<sup>17</sup> by spark source mass spectroscopy. A typical analysis for a hot pressed specimen and one powder lot is also shown in Table I. This analysis illustrates a more conservative statement of purity and demonstrates that comparison between analytical techniques is often difficult. For example, the Ca, Si and Na analyses show a considerable higher impurity concentration for both the powder and hot pressed specimen. It appears that Fe and Zn are introduced during consolidation and Cl, S and Na are volatilized during the consolidation process. Total impurity concentrations were actually lower in the fabricated sample. Analyses conducted under identical conditions are required for a well-founded discussion on relative purity of powders. Thus, it is with some reservation that the order of increasing purity is stated as SH194, SH182 and M10. Powder Lot M10 is still



#7680 (a) 1500X



A

B

#70687 (b) 1500X

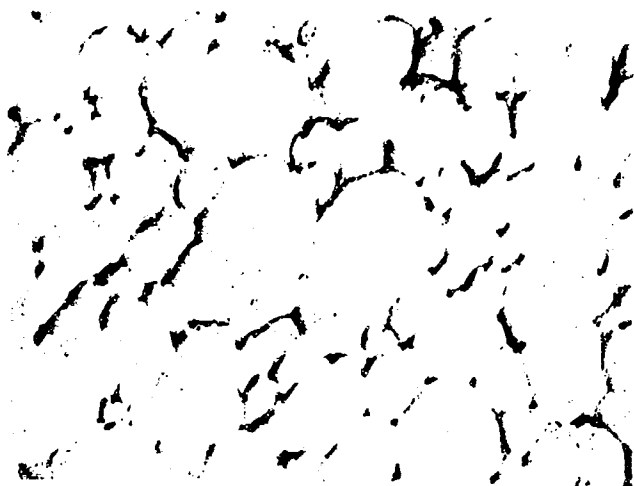


C

#70585 (c) 1500X

Figure 9. Microstructure Evolution of  $Mg(OH)_2$  Derived  $MgO$  at (a) 69% Density, (b) 92.5% Density, and (c) 99.5% Density.

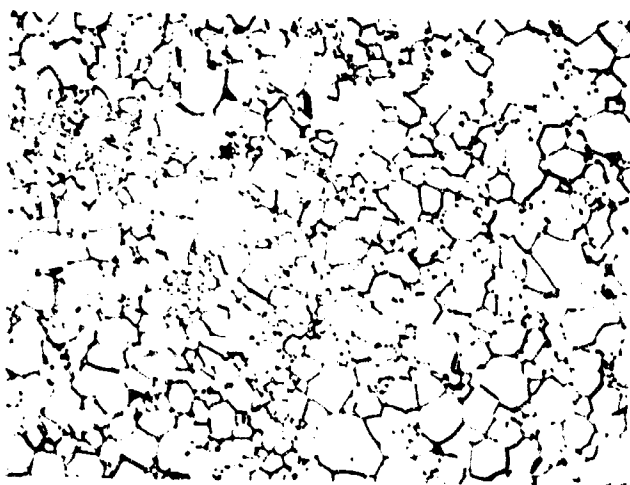
Hot Pressing Conditions  
and Results



#70693

15,000X

Honeywell - M10  
1150°C - 15 Kpsi - 90 min.  
3.551 gm/cc - 0.5  $\mu$ m grain  
intercept



#5412-5

500X

Honeywell - M10  
1250°C - 15 Kpsi - 90 min.  
3.585 gm/cc - 6  $\mu$ m grain  
intercept

Figure 10. Microstructure of Two MgO Samples Produced from  $MgCO_3$  Derived Powder.

TABLE II  
IMPURITY ANALYSIS FOR MAGNESIA BASE POWDER LOTS

<u>Element</u>	<u>Supplier Emission Spectrography Analysis</u>			<u>Spark Source Analysis</u>	
	<u>Lot SH194*</u>	<u>Lot SH182*</u>	<u>M-10** (16)</u>	<u>Lot SH182</u>	<u>Hot Pressed Sample 1330 (from Lot SH-182 Powder)</u>
Al	1	1	50	4	4
Ca	1	1	200	100	100
Cl				10	3
Cu	1	1	8	5	3
S				130	10
Au	1	ND		1	1
Zn				3	20
Fe	10	10		4	20
Pl	ND	30		4	0.6
Si	1	ND	150	150	150
Mn	ND	5		1	1
Na	1	1		1500	40

\* United Mineral  
\*\*Honeywell

thought to be a factor of ten more pure than that used for many experimental research programs<sup>3,4,5,17</sup> where problems with grain boundary phases have been encountered.

#### 4.4 Grain Growth

Preliminary grain growth studies were conducted with  $Mg(OH)_2$  (Lot SH 194) derived MgO hot pressed at  $1450^{\circ}C$  which possessed a starting grain intercept of  $34.2 \mu m$ . Pressing at this temperature achieved a normal grain size distribution, but the large grain size precluded growth studies at low temperatures. A series of runs were conducted at  $1610^{\circ}C$  and these were combined with data collected earlier<sup>17</sup> for analysis.

Specimens were cut from a single sample, polished and etched. A particular location in the sample was mapped and grain intercepts were measured. The grain sizes reported are average grain intercepts. Specimens were contained in a closed high purity  $Al_2O_3$  crucible and were in contact with a hot pressed MgO setter plate fabricated from the same high purity starting material used in the study. Samples were inserted and withdrawn from an isothermal air furnace for the prescribed times. They were ground to remove any surface effects. After repolishing and etching, final grain sizes were measured in the same location in which the initial grain sizes were measured.

Grain growth data plotted according to equation (1) is given in Figure 11. Comparative data of Spriggs et al<sup>5</sup> and Gordon et al<sup>17</sup> is also illustrated. Data at  $1525, 1610^{\circ}C$  and that of Gordon et al, exhibit a significant decay in growth rate. Plotting the data using different times exponents,  $n$ , in the relation  $D^n - D_0^n = k t$  at values of  $n$  up to 4 did not fit all of the data although the fit was moderately good at  $n = 4$ .

The microstructures were examined carefully after annealing for the development of pores and their location. Figure 12 illustrates the structure after annealing for about 1000 minutes at three temperatures;  $1300, 1525$  and  $1610^{\circ}C$ . These are to be compared with the starting microstructure illustrated in Figure 7c. The pore level increases with increasing annealing temperature. In general, pores are located at grain boundaries; however, a number of pores have separated from the boundaries and are located within grains.

#### 4.5 Discussion

The decomposition of  $Mg(OH)_2$  is accompanied by a 55% decrease in molar volume. Early researchers reported that upon decomposition MgO had its cubic  $\{110\}$  and  $\{111\}$  planes parallel to the prism and basal planes of the hexagonal brucite lattice, respectively. Gordon and Kingery<sup>15</sup> observed separate diffraction spots for the (110) brucite and (220) magnesium oxide planes. The positions of the (110) and (100) brucite never change, but only diminished in intensity while the (220) planes of magnesium oxide shifted from a value larger than the listed ASTM d spacing to the predicted value as the decomposition progressed. They describe the process as a nucleation and growth mechanism in which the magnesium oxide nuclei form coherently with the brucite matrix introducing large strains and causing extensive fracturing of the platelets. Exactly the same results were observed in the present electron diffraction studies. Further, the existence of rod-like crystallites (Figure 3b) suggested that a preferred growth was dominant under static low temperature growth conditions. A different mode of preferred growth was evident in the high

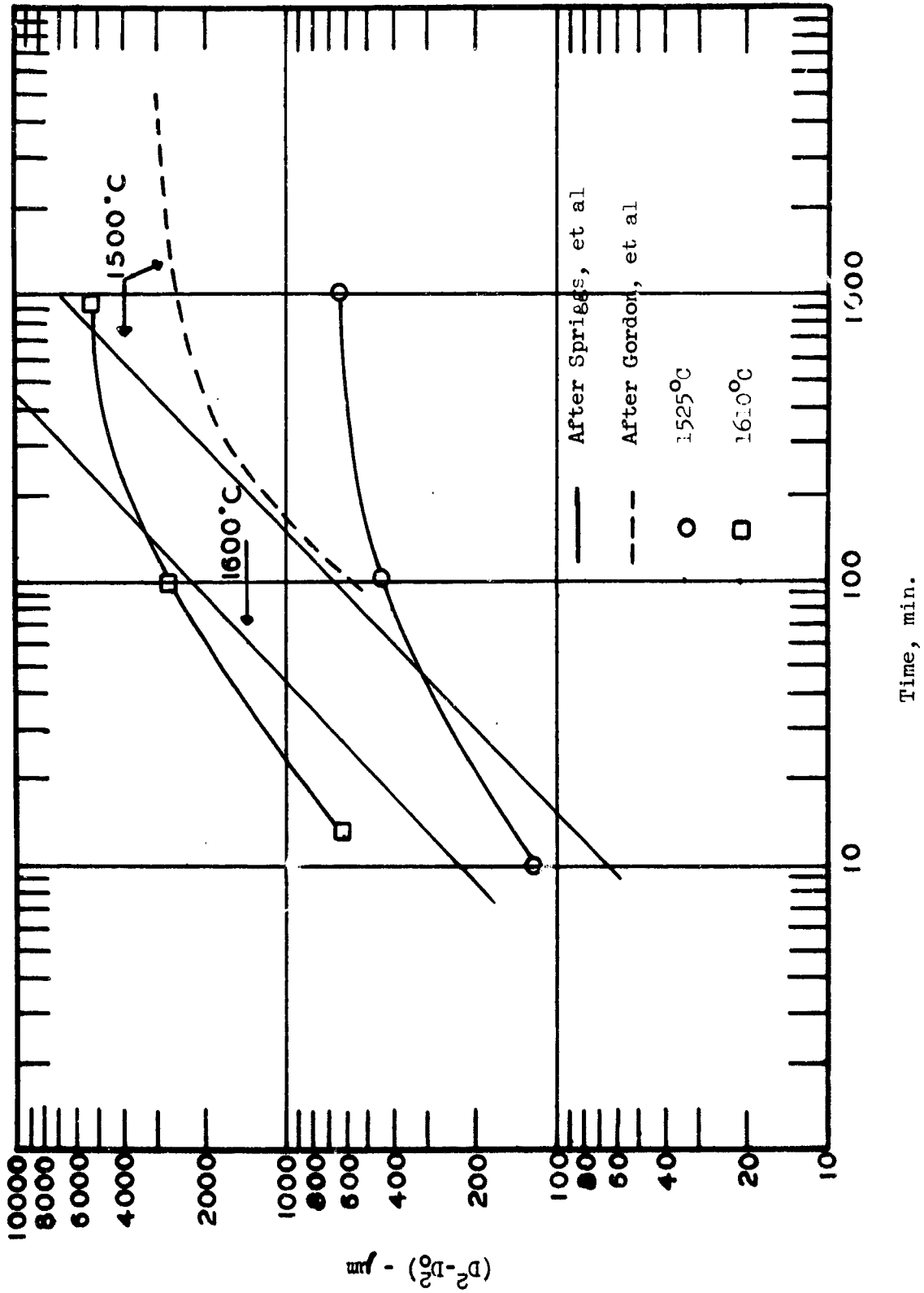
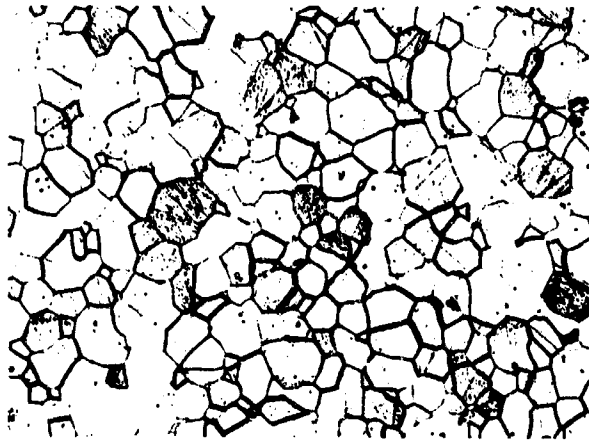
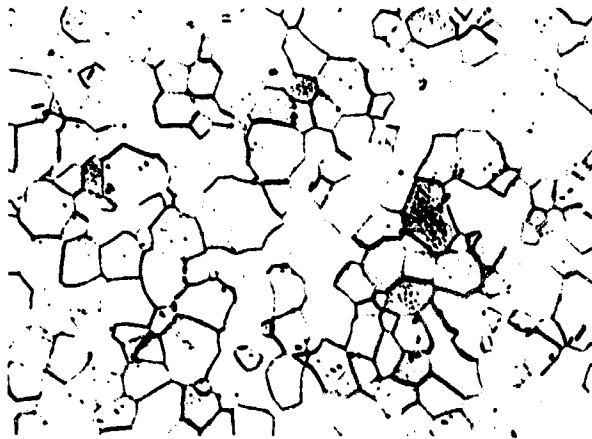


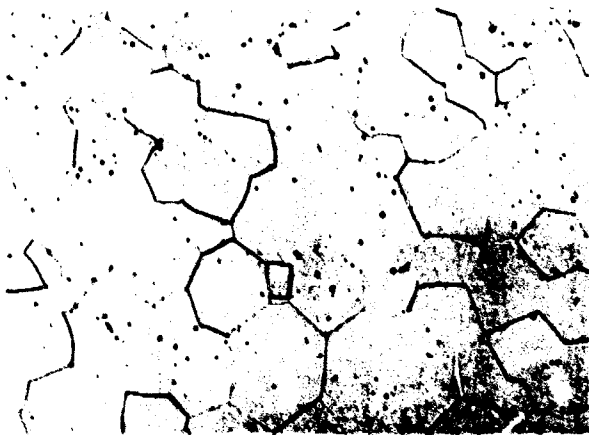
Figure 11. Grain Growth in High Purity MgO and Comparison with Literature Values.



#4900-3 (a) 100X



#5055-1 (b) 100X



#5406-4 (c) 100X

Figure 12. Microstructure after Approximately 1000 Minutes Annealing at (a) 1300°C, (b) 1525°C, and (c) 1610°C.

temperature calcinations. In the high temperature case orthogonally equivalent preferred growth rates resulted in a cubic habit.

The coherent nucleation of MgO within the Mg(OH)<sub>2</sub> platelet results in crystallites perfectly oriented one to another. Because of the preferred growth rate, crystallite growth during calcination results in somewhat larger crystallites within the brucite relic agglomerates than those crystallites which have broken away from their parent relic structures. This size difference is not large in the powder stage as witnessed by the fact that a log normal size distribution was obtained for the 1200°C-1 hr calcine. However, it appears that the enhanced growth within agglomerates becomes important in microstructure development. As shown in Figure 9c, grain boundaries sweep through entire agglomerates leaving very large grains. Crystallites that broke away from their agglomerate parent or small agglomerates arrive at quite different grain sizes upon reaching full density. Clearly, abnormal grain growth conditions arose early in the densification cycle. Somewhat analogous results occurred in sintering studies on very fine yttria-stabilized zirconia.<sup>18</sup> The crystallite-agglomerate explanation for the duplex grain structure development appears more reasonable than one based on retained volatiles which was the initial hypothesis. The fact that dynamic vacuum calcines as high as 1200°C still resulted in duplex microstructures strongly suggest that volatiles are not leading to retarded or accelerated growth. Also, of course, the direct observation of microstructure evolution points to a crystallite agglomerate interaction.

MgCO<sub>3</sub> undergoes a 50% reduction in molal volume during conversion to MgO. Although the decomposition mechanism and kinetics are not well known, this larger reduction undoubtedly results in more displacement between crystallites than in the case of Mg(OH)<sub>2</sub> derived powder. It is unlikely that coherent nucleation occurs as the cube-shaped crystallites are randomly oriented to one another (Figure 5). Thus, preferred growth directions do not result in grain boundaries rapidly sweeping through an agglomerate relic. This apparently accounts for grain sizes a factor of 30-40 smaller compared with Mg(OH)<sub>2</sub> derived powder processed under identical conditions. Possible chemical effects cannot be completely discounted, however. A particular impurity species may be present in this 99.99+% pure Honeywell MgO that acts as a grain growth retardation agent. Earlier Avco studies with 99.4% pure MgO (MgCO<sub>3</sub> derived) yielded 6 μm grain intercept after 240 minutes at 1250°C which supports the present relative order of grain size versus hot pressing cycle versus precursor. Complete satisfaction on this point must await a future critical experiment where chemistries are kept as close as possible for MgCO<sub>3</sub> and Mg(OH)<sub>2</sub> derived MgO.

A particularly interesting and surprising result of this study was the development of a normal grain size distribution in Mg(OH)<sub>2</sub> derived material hot pressed at 1450°C. Usually upon achieving abnormal grain conditions, the abnormal structure becomes more exaggerated with increasing growth unless some event such as primary recrystallization initiates a new generation of grains.<sup>13</sup> Based on the interrupted densification microstructure studies, it appears that an abnormal intermediate structure developed into a normal structure upon further growth. Hard evidence to explain this result is lacking but one possible mechanism may be obtained by evaluating the work of Brook<sup>14</sup> as discussed earlier. Grain growth up to the point illustrated in Figure 7b

could be boundary controlled, but at this point the large grains possess a grain size/pore size ratio such that further growth becomes slowed and falls into the pore control regime. Meanwhile the small grains continue to be boundary controlled (a faster process) affording them the opportunity to catch up to the large grains in size. Pores are not readily discernable in Figure 7c, but further heat treatment of this type of material (Figure 12) demonstrates the presence of a limited porosity.

The grain growth kinetic studies demonstrated a marked decay in growth at long times which was similar to the results of Gordon. The decay occurred at different sizes for the two temperatures. The decay is thought to be related to the competing processes for grain growth control; 1) boundary mobility controlled either by pure intrinsic diffusion or influenced by impurity drag, or 2) pore mobility controlled (again either controlled by intrinsic or impurity influenced diffusion). The growth kinetics are likely to change from square to cube dependence when the controlling process change from boundary to pore diffusion controlled.<sup>14</sup> Further decay beyond  $n = 3$  was observed by Gordon et al<sup>7</sup> when pore separation occurred. Figure 12 does illustrate pore entrapment, thus the present results agree with those of Gordon et al. Pore separation apparently leads to abnormal grain growth as witnessed by the disproportionate number of grains which have greater or fewer number of sides than the idealized number (6) as shown in Figure 12. This may occur because the pores become disassociated from the grain boundary non-uniformly breaking away first from one boundary and then another. As pores break away from a boundary, that boundary becomes free to migrate at a faster rate than boundaries that are still bound to pores. This could easily lead to the development of 7 or more sides on a grain and the onset of abnormal growth.

The initial growth rate was slightly higher than that for the study of Spriggs et al.<sup>5</sup> This could be a result of less impurity drag for the high purity material compared with that of Spriggs et al (about 99.4% pure MgO). As noted above, the initial portion of the curve was thought to be boundary migration controlled. As growth became pore migration controlled, the growth rate decayed below that of Spriggs et al. The material of Spriggs et al did not develop porosity during the high temperature anneals.

The cause of pore development in one material and absence in another is uncertain; however, several comments are appropriate. The material of Spriggs et al was vacuum hot pressed in an  $Al_2O_3$  die while the material of Gordon et al was vacuum hot pressed in molybdenum alloy dies, and the material of the present study vacuum hot pressed in graphite dies. Some argument might be forwarded for graphite leading to a CO entrapment that could lead to pore coalescence upon annealing, but since similar results were obtained for the molybdenum die prepared material, this does not appear to be the common factor. The development of 0.1 to 0.5% porosity is in fact quite common in annealing and grain growth of hot pressed material. This is thought to arise from two causes; 1) expansion of micro-pores that were constrained under hydrostatic loads during hot pressing and 2) coalescence of gas molecules adsorbed on grain boundaries. The best known exception to statement about annealing causing grain growth is transparent polycrystalline MgO produced by the process incorporating ~ 1% LiF. Annealing is part of this process and yields very transparent material as LiF diffuses via the grain boundaries to the surface and evaporates. Part of this process may be to sweep potential

pore forming gas molecules to the surface. This point is brought out because recent studies<sup>17</sup> of 99.4% MgO (the chemistry of the Spriggs et al study) have shown that a very thin grain boundary phase exists. Electron diffraction identified this phase as  $\text{Na}_6\text{Al}_4\text{Si}_4\text{O}_{17}$ . It is suggested that this phase behaves much like  $\text{LiF}$ , sweeping potential pore forming molecules to the surface or keeping them in solid solution. This might explain the absence of porosity in the study of Spriggs et al and account for the major kinetic difference as compared with the studies of Gordon et al and the present authors.

## V. CONCLUSIONS

1. Brucite decomposes by the coherent nucleation of MgO leaving crystallographically oriented MgO crystallites within an agglomerate which is a relic of the  $\text{Mg}(\text{OH})_2$  crystal. Preferred growth directions resulted in a rod structure when calcined at  $375^\circ\text{C}$  and a cube when calcined at  $900^\circ\text{C}$  and above.
2. Abnormal grain growth develops at 70% density in the vacuum hot pressing consolidation cycle leading to duplex grain structures for  $\text{Mg}(\text{OH})_2$  derived powder. It appears that the oriented crystallites within an agglomerate grow extremely rapidly due to the "special" nature of the boundary. Both static and vacuum dynamic calcined material give the same results. Hot pressing at higher temperatures ( $1450^\circ\text{C}$ ) than required for full densification ( $1150^\circ\text{C}$ ) develops a normal grain structure. This grain size development is thought to be related to the competing processes of boundary and pore control on grain growth.
3. The purity of the fabricated specimens were equal to or greater than the powder. Fe and Zn were introduced during pressing while Ca, Si and Na concentrations were lowered. The purity of the best samples counting anions (except  $\text{OH}^-$ ) and cations were 99.965% MgO.
4. Magnesium carbonate derived MgO also yields crystallites with a cubic growth habit, but the crystallites within an agglomerate are unoriented with respect to one another.
5. Vacuum hot pressed bodies from  $\text{MgCO}_3$  derived powder have normal grain size distributions when hot pressed at  $1150^\circ\text{C}$  and a factor of 30 smaller grain size than  $\text{Mg}(\text{OH})_2$  derived powder. Several explanations for this difference were discussed, but the most strongly forwarded was the absence of rapid growth due to unoriented crystallites in  $\text{MgCO}_3$  derived agglomerates.
6. Grain growth rates decayed during anneals at  $1526^\circ\text{C}$  and  $1610^\circ\text{C}$ . This was due to the transition from boundary control to pore control to abnormal grain growth since porosity became apparent during the course of the anneals. A hypothesis was forwarded that earlier results on 99.4% MgO followed the normal square time dependence due to the action of a very thin grain boundary phase sweeping out pores or their nuclei and hence, the lack of pore control throughout the anneal.

VI. REFERENCES

1. M.H. Leipold, J. Am. Ceram. Soc., 49, 498 (1966).
2. B.J. Wuensch and T. Vasilos, J. Am. Ceram. Soc., 49, 433 (1966).
3. R.J. Stokes, J. Am. Ceram. Soc., 48, 60 (1965).
4. A.U. Daniels, Jr., R.C. Lowrie, Jr., R.L. Gibby and I. Cutler, J. Am. Ceram. Soc., 45, 282 (1962).
5. R.M. Spriggs, L.A. Brissette and T. Vasilos, J. Am. Ceram. Soc., 47, 417 (1964).
6. G.C. Nicholson, J. Am. Ceram. Soc., 49, 47 (1966).
7. R.S. Gordon, D.D. Marchant and G.W. Hollenberg, J. Am. Ceram. Soc., 53, 399 (1970).
8. B.J. Wuensch and T. Vasilos, NBS Spec. Publ. 296, 95 (1968).
9. D. Turnbull, Trans. A.I.M.E., 191, 661 (1951).
10. W.D. Kingery and E. Fraricis, J. Am. Ceram. Soc., 48, 546 (1965).
11. F.A. Nichols, J. Appl. Phys., 37, 4599 (1966).
12. J.W. Cahn, Acta. Met., 10, 789 (1962).
13. M. Hillert, Acta. Met., 13, 227 (1965).
14. R.J. Brook, J. Am. Ceram. Soc., 52, 56 (1969).
15. R.S. Gordon and W.D. Kingery, J. Am. Ceram. Soc., 49, 654 (1966).
16. S.M. Copley, J.A. Pask, J. Am. Ceram. Soc., 48, 636 (1965).
17. W.H. Rhodes, P.F. Jahn and P.L. Burnett, Contract N00019-68-C-0108, AVATD-0121-69-CR, June 1969.
18. W.H. Rhodes and R.M. Haag, Contract F33615-67-C-1693, AFML-TR-70-209.



UNCLASSIFIED

Security Classification

14 KEY WORDS	LINK A		LINK B		LINK C	
	ROLE	WT	ROLE	WT	ROLE	WT
Magnesium oxide Grain growth High purity Hot pressing						

## INSTRUCTIONS

1. **ORIGINATING ACTIVITY:** Enter the name and address of the contractor, subcontractor, grantee, Department of Defense activity or other organization (corporate author) issuing the report.

2a. **REPORT SECURITY CLASSIFICATION:** Enter the overall security classification of the report. Indicate whether "Restricted Data" is included. Marking is to be in accordance with appropriate security regulations.

2b. **GROUP:** Automatic downgrading is specified in DoD Directive 5200.10 and Armed Forces Industrial Manual. Enter the group number. Also, when applicable, show that optional markings have been used for Group 3 and Group 4 as authorized.

3. **REPORT TITLE:** Enter the complete report title in all capital letters. Titles in all cases should be unclassified. If a meaningful title cannot be selected without classification, show title classification in all capitals in parenthesis immediately following the title.

4. **DESCRIPTIVE NOTES:** If appropriate, enter the type of report, e.g., interim, progress, summary, annual, or final. Give the inclusive dates when a specific reporting period is covered.

5. **AUTHOR(S):** Enter the name(s) of author(s) as shown on or in the report. Enter last name, first name, middle initial. If military, show rank and branch of service. The name of the principal author is an absolute minimum requirement.

6. **REPORT DATE:** Enter the date of the report as day, month, year, or month, year. If more than one date appears on the report, use date of publication.

7a. **TOTAL NUMBER OF PAGES:** The total page count should follow normal pagination procedures, i.e., enter the number of pages containing information.

7b. **NUMBER OF REFERENCES:** Enter the total number of references cited in the report.

8a. **CONTRACT OR GRANT NUMBER:** If appropriate, enter the applicable number of the contract or grant under which the report was written.

8b, 8c, & 8d. **PROJECT NUMBER:** Enter the appropriate military department identification, such as project number, subproject number, system numbers, task number, etc.

9a. **ORIGINATOR'S REPORT NUMBER(S):** Enter the official report number by which the document will be identified and controlled by the originating activity. This number must be unique to this report.

9b. **OTHER REPORT NUMBER(S):** If the report has been assigned any other report numbers (either by the originator or by the sponsor), also enter this number(s).

10. **AVAILABILITY/LIMITATION NOTICES:** Enter any limitations on further dissemination of the report, other than those

imposed by security classification, using standard statements such as:

- (1) "Qualified requesters may obtain copies of this report from DDC."
- (2) "Foreign announcement and dissemination of this report by DDC is not authorized."
- (3) "U. S. Government agencies may obtain copies of this report directly from DDC. Other qualified DDC users shall request through \_\_\_\_\_."
- (4) "U. S. military agencies may obtain copies of this report directly from DDC. Other qualified users shall request through \_\_\_\_\_."
- (5) "All distribution of this report is controlled. Qualified DDC users shall request through \_\_\_\_\_."

If the report has been furnished to the Office of Technical Services, Department of Commerce, for sale to the public, indicate this fact and enter the price, if known.

11. **SUPPLEMENTARY NOTES:** Use for additional explanatory notes.

12. **SPONSORING MILITARY ACTIVITY:** Enter the name of the departmental project office or laboratory sponsoring (paying for) the research and development. Include address.

13. **ABSTRACT:** Enter an abstract giving a brief and factual summary of the document indicative of the report, even though it may also appear elsewhere in the body of the technical report. If additional space is required, a continuation sheet shall be attached.

It is highly desirable that the abstract of classified reports be unclassified. Each paragraph of the abstract shall end with an indication of the military security classification of the information in the paragraph, represented as (TS), (S), (C), or (U).

There is no limitation on the length of the abstract. However, the suggested length is from 150 to 225 words.

14. **KEY WORDS:** Key words are technically meaningful terms or short phrases that characterize a report and may be used as index entries for cataloging the report. Key words must be selected so that no security classification is required. Identifiers, such as equipment model designation, trade name, military project code name, geographic location, may be used as key words but will be followed by an indication of technical context. The assignment of links, rules, and weights is optional.

UNCLASSIFIED

Security Classification

UNCLASSIFIED

Security Classification

DOCUMENT CONTROL DATA - R&D		
<i>(Security classification of title, body of abstract and indexing annotation must be entered when the overall report is class'fied)</i>		
1. ORIGINATING ACTIVITY (Corporate author)		2a. REPORT SECURITY CLASSIFICATION
Avco Corporation Systems Division Lowell, Massachusetts		Unclassified
3. REPORT TITLE		2b. GROUP
Relation Between Particulate Chemistry and Ceramic Properties		
4. DESCRIPTIVE NOTES (Type of report and inclusive dates)		
5. AUTHOR(S) (Last name, first name, initial)		
6. REPORT DATE	7a. TOTAL NO. OF PAGES	7b. NO. OF REFS
8a. CONTRACT OR GRANT NO.	8b. ORIGINATOR'S REPORT NUMBER(S)	
a. PROJECT NO.	AVSD-0024-71-CR	
c.	8c. OTHER REPORT NO(S) (Any other numbers that may be assigned this report)	
d.		
10. AVAILABILITY/LIMITATION NOTICES		
11. SUPPLEMENTARY NOTES		12. SPONSORING MILITARY ACTIVITY
13. ABSTRACT Concl'd		
<p>normal square dependence due to the transition from boundary control to pore control and then to abnormal grain growth resulting from the critical relations between grain size and pore size (the 0.1 to 0.4% porosity only became apparent during the anneals). A discussion and explanation of the various grain growth studies in MgO is included.</p>		

DD FORM 1473  
1 JAN 64

UNCLASSIFIED

Security Classification

Security Classification

14	KEY WORDS					
	LINK A		LINK B		LINK C	
	ROLE	WT	ROLE	WT	ROLE	WT

**INSTRUCTIONS**

1. **ORIGINATING ACTIVITY:** Enter the name and address of the contractor, subcontractor, grantee, Department of Defense activity or other organization (*corporate author*) issuing the report.
- 2a. **REPORT SECURITY CLASSIFICATION:** Enter the overall security classification of the report. Indicate whether "Restricted Data" is included. Marking is to be in accordance with appropriate security regulations.
- 2b. **GROUP:** Automatic downgrading is specified in DoD Directive 5200.10 and Armed Forces Industrial Manual. Enter the group number. Also, when applicable, show that optional markings have been used for Group 3 and Group 4 as authorized.
3. **REPORT TITLE:** Enter the complete report title in all capital letters. Titles in all cases should be unclassified. If a meaningful title cannot be selected without classification, show title classification in all capitals in parenthesis immediately following the title.
4. **DESCRIPTIVE NOTES:** If appropriate, enter the type of report, e.g., interim, progress, summary, annual, or final. Give the inclusive dates when a specific reporting period is covered.
5. **AUTHOR(S):** Enter the name(s) of author(s) as shown on or in the report. Enter last name, first name, middle initial. If military, show rank and branch of service. The name of the principal author is an absolute minimum requirement.
6. **REPORT DATE:** Enter the date of the report as day, month, year; or month, year. If more than one date appears on the report, use date of publication.
- 7a. **TOTAL NUMBER OF PAGES:** The total page count should follow normal pagination procedures, i.e., enter the number of pages containing information.
- 7b. **NUMBER OF REFERENCES:** Enter the total number of references cited in the report.
- 8a. **CONTRACT OR GRANT NUMBER:** If appropriate, enter the applicable number of the contract or grant under which the report was written.
- 8b, 8c, & 8d. **PROJECT NUMBER:** Enter the appropriate military department identification, such as project number, subproject number, system numbers, task number, etc.
- 9a. **ORIGINATOR'S REPORT NUMBER(S):** Enter the official report number by which the document will be identified and controlled by the originating activity. This number must be unique to this report.
- 9b. **OTHER REPORT NUMBER(S):** If the report has been assigned any other report numbers (*either by the originator or by the sponsor*), also enter this number(s).
10. **AVAILABILITY/LIMITATION NOTICES:** Enter any limitations on further dissemination of the report, other than those

imposed by security classification, using standard statements such as:

- (1) "Qualified requesters may obtain copies of this report from DDC."
- (2) "Foreign announcement and dissemination of this report by DDC is not authorized."
- (3) "U. S. Government agencies may obtain copies of this report directly from DDC. Other qualified DDC users shall request through \_\_\_\_\_."
- (4) "U. S. military agencies may obtain copies of this report directly from DDC. Other qualified users shall request through \_\_\_\_\_."
- (5) "All distribution of this report is controlled. Qualified DDC users shall request through \_\_\_\_\_."

If the report has been furnished to the Office of Technical Services, Department of Commerce, for sale to the public, indicate this fact and enter the price, if known.

11. **SUPPLEMENTARY NOTES:** Use for additional explanatory notes.

12. **SPONSORING MILITARY ACTIVITY:** Enter the name of the departmental project office or laboratory sponsoring (*paying for*) the research and development. Include address.

13. **ABSTRACT:** Enter an abstract giving a brief and factual summary of the document indicative of the report, even though it may also appear elsewhere in the body of the technical report. If additional space is required, a continuation sheet shall be attached.

It is highly desirable that the abstract of classified reports be unclassified. Each paragraph of the abstract shall end with an indication of the military security classification of the information in the paragraph, represented as (TS), (S), (C), or (U).

There is no limitation on the length of the abstract. However, the suggested length is from 150 to 225 words.

14. **KEY WORDS:** Key words are technically meaningful terms or short phrases that characterize a report and may be used as index entries for cataloging the report. Key words must be selected so that no security classification is required. Identifiers, such as equipment model designation, trade name, military project code name, geographic location, may be used as key words but will be followed by an indication of technical context. The assignment of links, rules, and weights is optional.